buildings

MDPI

Article

Experimental Investigation on Shear Behavior of Non-Stirrup UHPC Beams under Larger Shear Span–Depth Ratios

Lifeng Zhang [1], Bowen Deng [1], Beini He [1], Haibo Jiang [1,*], Jie Xiao [1], Yueqiang Tian [2] and Junfa Fang [3]

[1] School of Civil and Transportation Engineering, Guangdong University of Technology, Guangzhou 510006, China; 3121003087@mail2.gdut.edu.cn (L.Z.); 3121003100@mail2.gdut.edu.cn (B.D.); 3222002779@mail2.gdut.edu.cn (B.H.); xiaojie2017@gdut.edu.cn (J.X.)
[2] Zhonglu Xincai (Guangzhou) Technology Co., Ltd., Guangzhou 511430, China; tian-t4@126.com
[3] Zhonglu Dura International Engineering Co., Ltd., Guangzhou 510430, China; fangjunfa2023@126.com
* Correspondence: hbjiang@gdut.edu.cn

Abstract: Due to the extraordinary mechanical properties of ultra-high-performance concrete (UHPC), the shear stirrups in UHPC beams could potentially be eliminated. This study aimed to determine the effect of beam height and steel fiber volume content on the shear behavior of non-stirrup UHPC beams under a larger shear span–depth ratio (up to 2.8). Eight beams were designed and fabricated including six non-stirrup UHPC beams and two comparing stirrup-reinforced normal concrete (NC) beams. The experimental results demonstrated that the steel fiber volume content could be a crucial factor affecting the ductility, cracking strength, and shear capacity of non-stirrup UHPC beams and altering their failure modes. Additionally, the height of the beam had a considerable effect on its shear resistance. French standard formulae were more accurate for the UHPC beams with larger shear span–depth ratios, PCI-2021 formulae greatly overestimated the shear capacity of UHPC beams with larger shear span–depth ratios, and Xu's formulae were more accurate for the steel fiber-reinforced UHPC beams with larger shear span–depth ratios. In summary, French standard formulae were the most suitable formulae for predicting the shear capacity of UHPC beams in this paper.

Keywords: shear behavior; ultra-high-performance concrete (UHPC); non-stirrup UHPC beams; large shear span-depth ratios; steel fiber volume content; beam height

check for updates

Citation: Zhang, L.; Deng, B.; He, B.; Jiang, H.; Xiao, J.; Tian, Y.; Fang, J. Experimental Investigation on Shear Behavior of Non-Stirrup UHPC Beams under Larger Shear Span–Depth Ratios. *Buildings* **2024**, *14*, 1374. https://doi.org/10.3390/buildings14051374

Academic Editor: George Morcous

Received: 12 March 2024
Revised: 7 May 2024
Accepted: 8 May 2024
Published: 11 May 2024

1. Introduction

Ultra-high-performance concrete (UHPC) is a cementitious composite consisting of cement, silica fume, quartz powder, fine aggregates, steel fibers, water reducer, and potable water. Given its excellent mechanical properties, superior workability, and durability, UHPC is considered one of the most promising engineering materials [1–4]. Additionally, UHPC exhibits excellent corrosion resistance and reliability due to its high compactness and self-healing ability [5,6]. Nowadays, it has been widely used in practical engineering, especially in bridge engineering [7–10]. Typical examples of its application include the first UHPC pedestrian bridge, Sherbrooke Quebec Bridge, in Canada in 1997; the first PI-shaped UHPC bridge, Jakway Park Bridge in Buchanan County, Missouri, USA; the world's first and largest UHPC arch bridge, Peace Bridge in South Korea; the world's first UHPC highway arch bridge, Wild Bridge in Austria; and the first and largest steel-UHPC truss foot bridge in China [11]. In addition, there is a significant body of research on the use of UHPC in bridge construction, covering various aspects such as waffle deck panels [12], segmental bridges [13,14], joints [15–17], connections [18,19], and steel-UHPC composite girders [20–24]. Nevertheless, the innovation of material has also resulted in high construction costs. In order to expand the application of UHPC in construction, it is necessary to identify cost-effective methods. In 2019, the inaugural prestressed non-stirrup UHPC girder bridge was constructed in China, reducing its own weight down to approximately half that of conventional NC beams. The exclusion of stirrups enhances the fluidity of UHPC, resulting in improved mechanical properties and provides a novel method to reduce costs.

In the context of normal concrete (NC) beam structures, dense stirrups are typically employed to resist shear forces [25,26]. The incorporation of steel fibers offers ultra-high tensile strength to the UHPC matrix, making it possible to eliminate the stirrups of UHPC beams [27,28]. Studies have shown that non-stirrup UHPC beams can withstand shear loads with a steel fiber volume content of 2% in the UHPC mixture [29]. Abbas et al. [30] discovered that the incorporation of steel fibers could enhance the post-cracking shear resistance of concrete beams. Amin et al. [31] demonstrated that steel fibers enabled better crack distribution, and that increasing the steel fiber volume content can significantly enhance the shear strength. However, when the steel fiber volume content exceeded a certain threshold, the mechanical properties of UHPC did not exhibit significant enhancements [32]. Furthermore, it is noteworthy that UHPC beams, which incorporated less than 0.5% volume of steel fiber, were unable to withstand as much shear load as the NC beams reinforced with stirrups [33]. Despite the extensive research conducted on the impact of steel fiber volume content on the shear behavior of non-stirrup UHPC beams, there remain numerous unresolved issues that require further investigation.

In general, steel fiber serves a similar function to stirrups in reinforcing concrete structures. By utilizing the ultra-high tensile strength of steel fiber in an UHPC matrix, it is possible to remove the stirrups to create slender, lighter, and more economical structural members. Currently, the majority of studies in the field of non-stirrup UHPC beams are concentrated on prestressing and thin-web I-section beams [34–37]. Jiang et al. [34] conducted four-point bending tests to investigate the shear performance of externally prestressed UHPC beams without stirrups. The study revealed that the shear strength decreased as the shear span–depth ratios increased. Furthermore, the study demonstrated that the cracking and shear strength of the beams would increase as the steel fiber volume content increased. Lee et al. [35] discovered that the non-stirrup UHPC I-girders exhibited excellent ductility, with the shear strength increasing progressively after the initial onset of cracks. The quantity and type of fibers incorporated in reactive powder concrete prestressed non-stirrup girders did not significantly influence the cracking load, but had a pronounced impact on the failure load and the rate of crack propagation [36]. It was demonstrated that the shear cracks in I-section prestressed non-stirrup UHPC beams were significantly distributed through the web prior to the formation of the critical crack [37]. In addition, numerous experimental and numerical studies have been conducted to investigate the influence of various parameters on the shear behavior of non-stirrup UHPC beams including the shear span–depth ratio, reinforcement ratio, and the volume content of steel fiber [38–41]. The shear behavior of non-stirrup UHPC beams was found to depend not only on the tensile strength of UHPC, but also on the prestressing force, fiber orientation, and shape of the cross-section [42]. The shear capacity of UHPC beams was found to be approximately 3.5 times greater than that of their counterparts on average. Furthermore, the reinforcement ratio had a negligible effect on the shear capacity of UHPC beams [43].

A larger shear span–depth ratio typically leads to a larger bridge span, which can effectively enhance the bridge's passability and reduce the number of piers required [44]. This simplifies the construction process and reduces construction difficulty. However, a larger shear span–depth ratio can also cause fatal problems to the bridge such as a remarkable reduction in its load-bearing capacity. External prestressing tendons can improve the shear strength of UHPC beams and make the cross-section of components smaller and thinner [45]. However, for small- and medium-span bridges, eliminating prestressing tendons is typically the preferred option due to the challenging environmental conditions, high cost, and difficulty in controlling the reverse arch.

In this study, non-stirrup UHPC beams were tested under a larger shear span–depth ratio at different steel fiber volume contents and beam heights to determine the shear behavior. Two NC beams were also employed for comparison. None of the tested beams were prestressed. To ascertain the accuracy of the French standard formula [46], PCI formula [47], and Xu's formula [48], the experimental results were compared with the calculated values.

2. Experimental Programs

2.1. Specimen Preparation

The aim of this research was to determine the effect of beam height and steel fiber volume content on the shear capacity of non-stirrup UHPC beams under a larger shear span–depth ratio (up to 2.8). Eight beams were designed and fabricated including six non-stirrup UHPC beams and two comparing stirrup-reinforced normal concrete (NC) beams. The dimensions and layouts of the beams are shown in Figure 1. The length of all tested beams (l) was designed to be 2100 mm, with a shear span-to-effective depth ratio (λ) of 2.8, where λ was calculated as $\lambda = a/h_0$, with a representing the shear span length of the beam and h_0 representing the effective depth of the beam. The specific values of a and h_0 are listed in Table 1. Furthermore, the cross-sections of the tested beams were rectangular, with a beam breadth *(b)* of 200 mm, and two beam heights (h) of 350 mm and 400 mm. To ensure shear failure mode, ribbed reinforcements with a diameter of 32 mm and a yield strength (f_y) of 419.2 MPa were used, along with double layers of longitudinal reinforcement placed at the bottom of the tested beams. The normal concrete (NC) beams employed double-leg stirrups that utilized 8 mm diameter ribbed reinforcements with a yielding strength of 412.0 MPa arranged at 100 mm intervals. The thickness of the concrete covering was 20 mm.

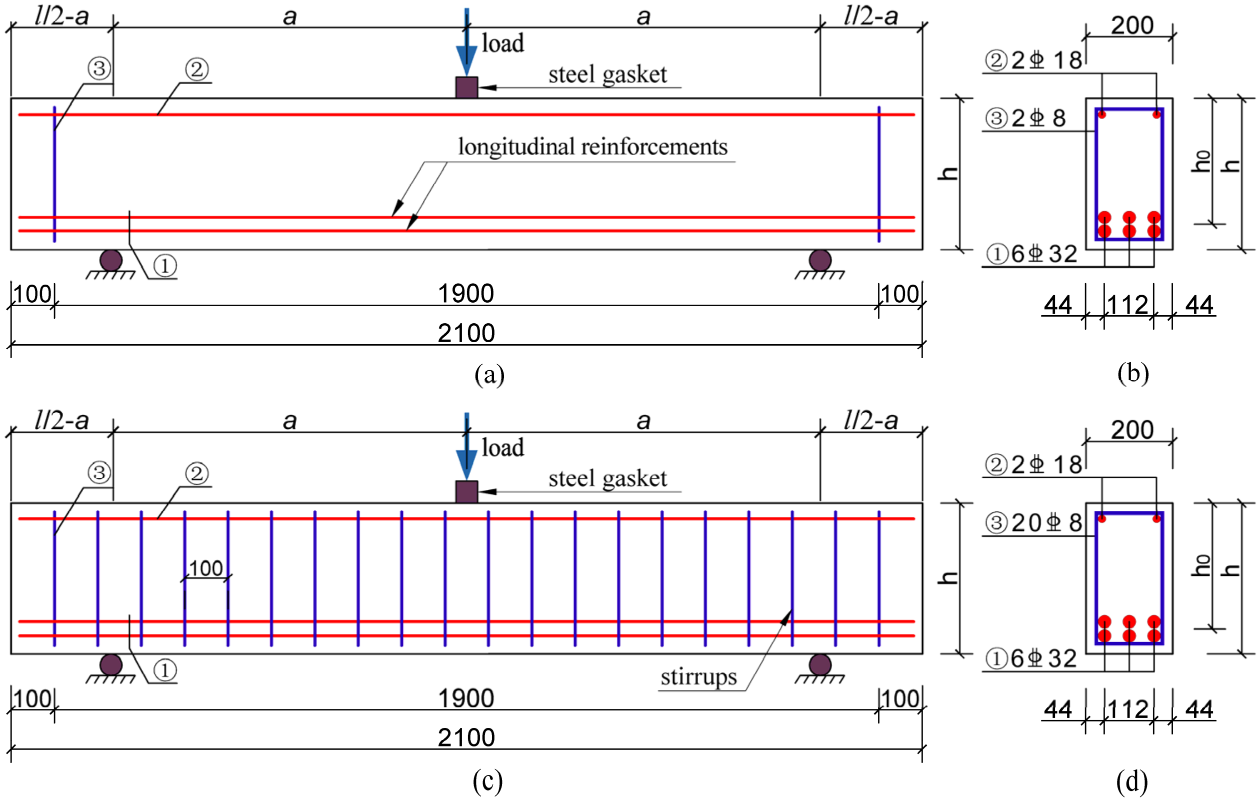

Figure 1. Dimensions and layouts of the tested beams (unit: mm). (**a**) Non–stirrup UHPC beams; (**b**) side elevation of (**a**); (**c**) stirrup–reinforced NC beams; and (**d**) side elevation of (**c**). Note: ① 6C32 indicates six HRB400 ribbed reinforcements with a 32 mm diameter, ② 2C18 indicates two HRB400 ribbed reinforcements with an 18 mm diameter, ③ 2C8 indicates two HRB400 8 mm diameter double–leg stirrups, and ③ 20C8 indicates twenty HRB400 8 mm diameter double–leg stirrups.

Table 1. Specimen nomenclature and experimental parameters.

No.	Specimens Nomenclature	Concrete Type	h/(mm)	Stirrup Ratio	Volume Content of Steel Fiber	h_0/(mm)	a/(mm)	λ
B1	U-H35-S0-V2.0	UHPC	350	0	2.0%	291	814.8	2.8
B2	U-H35-S0-V1.5	UHPC	350	0	1.5%	291	814.8	2.8
B3	U-H35-S0-V0	UHPC	350	0	0	291	814.8	2.8
B4	U-H40-S0-V2.0	UHPC	400	0	2.0%	341	954.8	2.8
B5	U-H40-S0-V1.5	UHPC	400	0	1.5%	341	954.8	2.8
B6	U-H40-S0-V0	UHPC	400	0	0	341	954.8	2.8
B7	N-H35-S1-V0	C40	350	0.584%	0	291	814.8	2.8
B8	N-H40-S1-V0	C40	400	0.599%	0	341	954.8	2.8

As shown in Figure 2, the processes of formwork fabricating, steel bar tying, and reinforcement cage laying were all carried out at the Structural Laboratory of Guangdong University of Technology in Guangzhou, China. The pouring work of the UHPC beam was carried out at the plant of the Zhonglu Dura International Engineering Co., Ltd. in Zhaoqing China. All equipment required for specimen preparation was sourced from China. Because of the excellent fluidity of UHPC, the tested UHPC beams were fabricated without vibration.

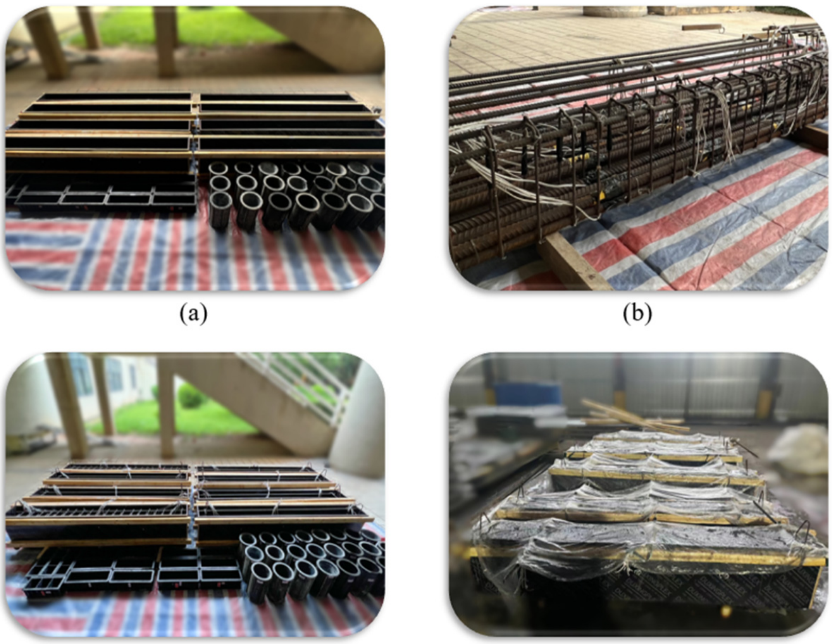

(a) (b) (c) (d)

Figure 2. Construction of the specimens. (**a**) Formwork fabricating; (**b**) steel bar tying; (**c**) reinforcement cages laying; (**d**) tested beam casting.

As shown in Table 1, the experimental variables encompass the type of concrete, beam height, with or without stirrups, and steel fiber volume content. To clearly indicate the variables, the specimens were labelled as U–H*–S*–V* or N–H*–S*–V*. The letter "U" represents ultra-high-performance concrete, while "N" represents normal concrete. The beam height is represented by 'H35′ and 'H40′ for 350 mm and 400 mm, respectively. "S1" and "S0" indicate whether the beams were constructed with or without stirrups, respectively. Additionally, "V2.0", "V1.5", and "V0" indicate the steel fiber volume contents of 2.0%, 1.5%, and "0", respectively. For instance, "U–H35–S0–V2.0" represents a 350 mm high UHPC beam without stirrups with a steel fiber volume content of 2.0%.

2.2. Test Setup and Instrumentation

To improve efficiency, three-point loading tests were performed on each specimen to evaluate the shear behavior of the non-stirrup UHPC beams, as shown in Figure 3. The specimens were subjected to a vertical concentrated load using an electro-hydraulic servo machine with a capacity of 10,000 kN. Each specimen was supported by two roller supports. Three linear vertical displacement transducers (LVDTs) were employed to monitor the deflections of the tested beams, which were positioned at the midspan of each beam and the locations of the roller supports, respectively. Figure 4 shows six groups of strain rosettes labelled A_1 to C_1 and A_2 to C_2, evenly distributed along the line extending from the loading point to the supports. Each strain rosette comprised three strain gauges, set at angles of 0°, 45°, and 90°, which were utilized to measure the principal strains. The longitudinal reinforcement strain and stirrup strain were quantified by the strain gauges affixed to the rebars. To ensure accurate measurements, the rebars were sanded smooth at the gauge location before applying the strain gauges. Furthermore, waterproof adhesive and anti-collision blocks were used to protect the strain gauges. The longitudinal reinforcements were labelled 1–3 and 4–6 from the south side to the north side of the double layer reinforcements, respectively, as shown in Figure 4c. The letters "N" and "S" indicate north and south, respectively. The strain gauges attached to the longitudinal reinforcements were labelled W_1–W_6, M_1–M_6, and E_1–E_6 from the west side to the east side. The letters "W", "M", and "E" indicate west, middle, and east, respectively. All data were collected using the JMTEST static collector including load force, beam deflection, longitudinal reinforcement strain, stirrup strain, and concrete strain. The detail of the layout of the strains and LVDTs can be seen in Figure 4.

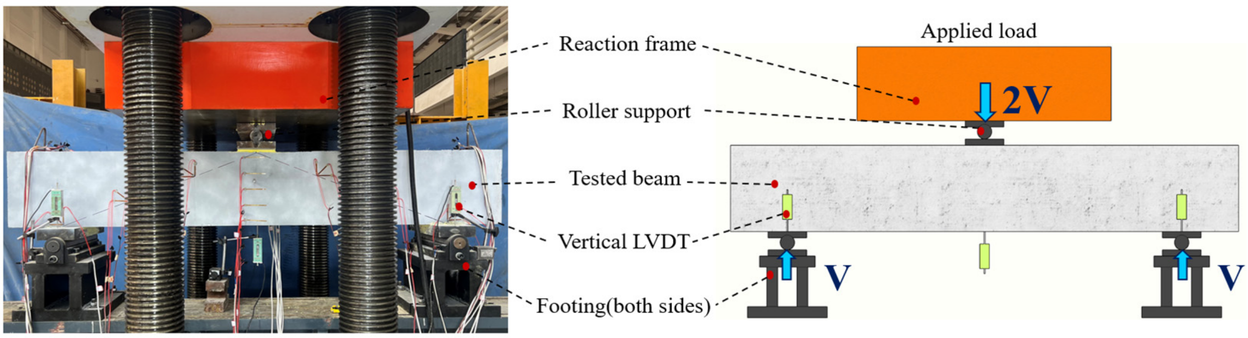

Figure 3. Experimental setup and instrumentation.

(**a**)

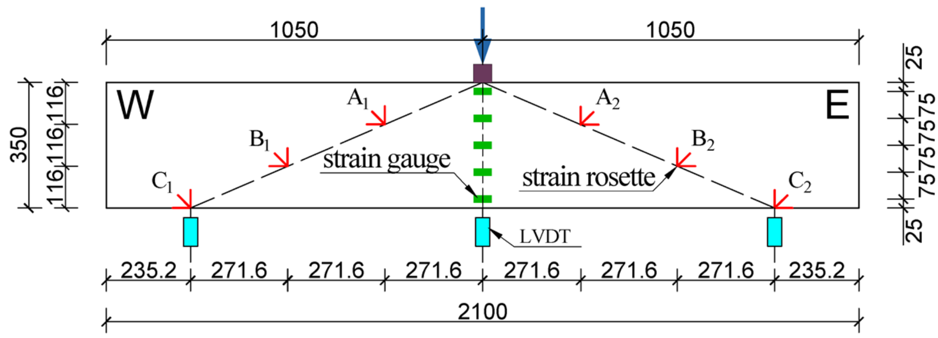

Figure 4. *Cont.*

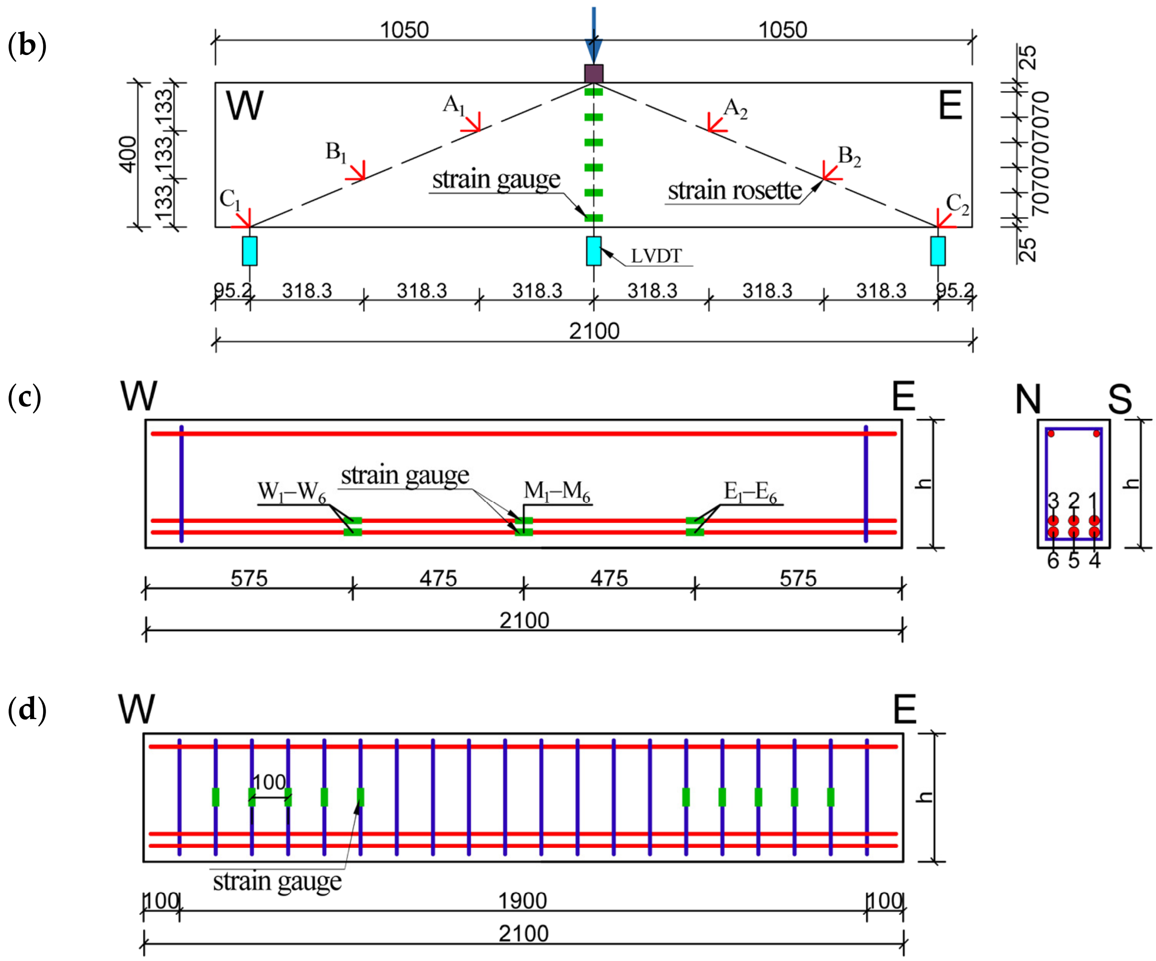

Figure 4. Layout of measuring points. (**a**) External measuring points of the 350 mm high tested beams; (**b**) external measuring points of the 400 mm high tested beams; (**c**) strain gauges of the longitudinal reinforcements; (**d**) strain gauges of the stirrups.

The loading protocol comprised two phases: the force-controlled phase and displacement-controlled phase. Before the shear diagonal cracks emerged, the loading was force controlled with an internal force of 50 kN. After that, the displacement-controlled phase was carried out at a loading rate of 0.1 mm/min. When the load was reduced to 60% of the peak load, the test was terminated. The schematic representation of the loading protocol is shown in Figure 5.

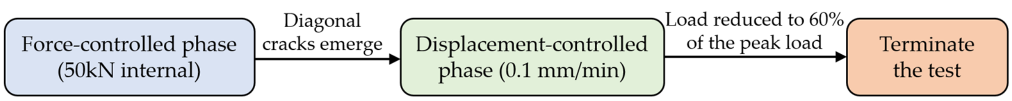

Figure 5. Schematic representation of the loading protocol.

2.3. Material Properties

The UHPC used in this study was provided by Zhonglu Dura International Engineering Co., Ltd. in Zhaoqing China, and was the same as the mixture used by Feng et al. [45]. The relevant equipment was source from China. A flow test was conducted and the slump flow diameter was 80 mm, as presented in Figure 6. The mechanical properties of the UHPC were subjected to rigorous testing including cubic compressive strength, axial compressive strength, splitting tensile strength, and flexural tensile strength.

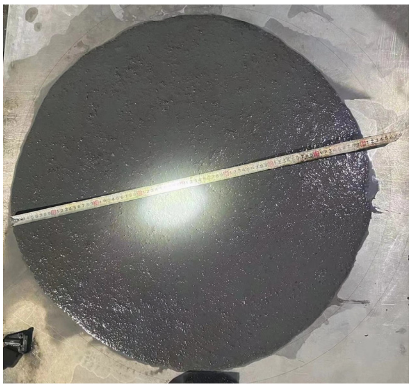

Figure 6. Results of the flow test.

In accordance with French standard NF P18-710 [46], the post-cracking strength can be determined by the following equation:

$$\sigma_{f1} = \frac{1}{w^*} \int_0^{w*} \sigma_f(w)dw \quad (1)$$

The post-cracking strength considering a fiber orientation factor (K) is calculated by:

$$\sigma_{f2} = \frac{\sigma_{f1}}{K} \quad (2)$$

The post-cracking strength for design is obtained from:

$$\sigma_{f3} = \frac{\sigma_{f1}}{K\gamma_{cf}} \quad (3)$$

where the post-cracking strength σ_f (w) is determined based on the crack opening w. In this study, a maximal crack width (w^*) of 0.3 mm, a fiber orientation factor (K) of 1.25, and a partial safety factor (γ_{cf}) of 1.3 were chosen, based on the recommended values of French standard NF P 18-470 [46].

As per the PCI report [47], the post-cracking residual strength f_{rr} is identified as the first peak cracking value, which is determined by:

$$f_{rr} = 0.375 f_{fu} \quad (4)$$

where f_{fu} is the flexural tensile strength.

In accordance with Xu's formula [48], the axial compressive strength f_c was determined from 300 mm × 100 mm × 100 mm prisms. Table 2 provides an overview of the properties of the UHPC utilized in this study. It should be noted that the ultimate flexural strength (f_{fu}) was affected by unknown reasons, which led to the f_{fu} of UHPC-2.0 being lower than the f_{fu} of UHPC-1.5.

Table 2. Basic mechanical properties of UHPC materials.

Concrete Type	Volume Content of Steel Fiber	f_{cu} (MPa)	f_c (MPa)	f_t (MPa)	σ_{f1} (MPa)	σ_{f2} (MPa)	σ_{f3} (MPa)	f_{fu} (MPa)	f_{rr} (MPa)
UHPC-0	0%	118.5	94.7	5.57	3.10	2.48	1.94	10.5	3.9
UHPC-1.5	1.5%	174.9	162.0	12.60	8.94	7.15	5.50	36.0	13.5
UHPC-2.0	2.0%	164.0	147.2	12.58	5.62	5.00	3.46	28.8	10.8
C40	0%	43.3	38.4	/	/	/	/	/	/

Notes: f_{cu} = cubic compressive strength; f_c = axial compressive strength; f_t = splitting tensile strength; σ_{f1} = tested post-cracking strength; σ_{f2} = post-cracking strength considering a fiber orientation factor (k) of 1.25; σ_{f3} = post-cracking strength for design; f_{fu} = flexural tensile strength; f_{rr} = post-cracking residual strength. σ_{f1}, σ_{f2}, and σ_{f3} were the inferred values according to f_{fu}.

Table 3 presents the test results for the mechanical properties of the stirrups and longitudinal reinforcements. The results were obtained by averaging the tested values of three randomly selected specimens, which were truncated from the rebars. The length of the specimens was 350 mm, and the calculated elastic modulus was assumed to be 2×10^5 MPa. The yield and ultimate strains of the rebars were measured by the strain gauges affixed to the rebars. The yield and ultimate strength of the rebars were derived based on the elastic modulus, yield strain, and ultimate strain [49]. All tests were conducted using an electro-hydraulic servo machine.

Table 3. Mechanical properties of rebars.

Specimens	Reinforcing Steel Type	Diameter (mm)	Yield Strength (MPa)	Ultimate Strength (MPa)	Yield Strain (%)	Ultimate Strain (%)
Stirrups	HRB400	8	412.0	621.1	0.23	13.22
Longitudinal reinforcements	HRB400	32	419.2	631.9	0.23	13.50

3. Experimental Results and Observation

3.1. Crack Patterns and Shear Failure Modes

All tested beams exhibited shear failures, specifically diagonal tension failure (DT), shear compression failure (SC), and diagonal compression failure (DC), as illustrated in Figure 7. Figure 8 shows the failure modes and crack patterns observed in all tested beams. Critical cracks are depicted using thick, solid lines, while areas of significant concrete damage are highlighted in bold black. DC failure occurred in the stirrup-reinforced NC beams, DT failure in the non-stirrup UHPC beams without steel fibers, and SC failure in the non-stirrup UHPC beams with steel fibers.

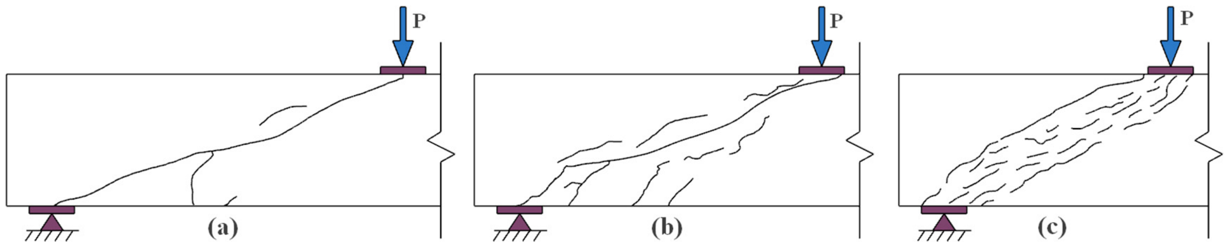

Figure 7. Types of shear failure. (**a**) Diagonal tension failure; (**b**) shear compression failure; (**c**) diagonal compression failure.

Specimens B1, B2, B4, and B5 exhibited characteristic patterns of shear compression failure. At the beginning of loading, flexural cracks emerged at the bottom of the tested beams. As the load approached a level between 35% and 55% of the peak load, the number of flexural cracks ceased to increase, and the existing flexural cracks gradually extended toward the loading point. Diagonal cracks were observed to emerge when the load reached a level between 31% and 61% of the peak load. Under increasing load, new diagonal cracks appeared, and eventually, a critical diagonal crack developed, which extended toward the loading point. When reaching the ultimate load, the concrete near the loading point was crushed.

In specimens B3 (Figure 8c) and B6 (Figure 8f), as soon as the diagonal cracks emerged in the shear span, the crack width rapidly increased and soon developed into critical diagonal cracks. Eventually, the two beams suddenly lost their load-bearing capacity and split in two, with flat failure surfaces and no concrete crushing. Therefore, it can be concluded that diagonal tension failure occurred at B3 and B6.

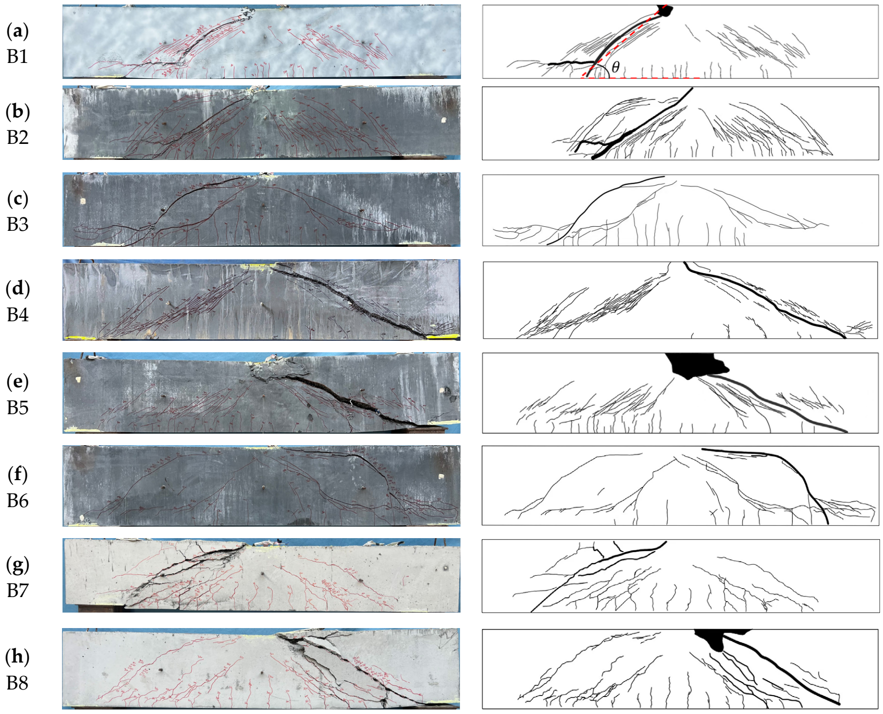

Figure 8. Crack pattern of each tested beam. (**a**) B1; (**b**) B2; (**c**) B3; (**d**) B4; (**e**) B5; (**f**) B6; (**g**) B7; and (**h**) B8.

In specimens B7 (Figure 8g) and B8 (Figure 8h), few cracks were observed until the load reached 40% of the ultimate load. As the load increased, several parallel diagonal cracks appeared, dividing the web of the beams into several inclined compression columns. After reaching the ultimate load, the tested beams were suddenly damaged. It can be concluded that the shear failure mode of B7 and B8 was diagonal compression damage.

It was especially noted that beams B1, B2, B4, and B5 also exhibited flexural failure due to the longitudinal rebar yielding, which concomitantly emerged with shear compression failure.

3.2. Experimental Results of the Tested Beams

Table 4 lists the experimental results of all of tested beams.

Table 4. Experimental results of all tested beams.

NO.	P_{cr} (kN)	σ_{cr} (MPa)	P_{ci} (kN)	v_{ci} (MPa)	P_u (kN)	V_u (kN)	τ_u (MPa)	Δ_u (mm)	$P_{failure}$ (kN)	$\Delta_{failure}$ (mm)	P_y (kN)	Δ_y (mm)	μ_Δ	θ	PCSR	Failure Pattern
B1	80	8.0	581	5.0	1340	670	11.5	7.53	986	9.30	1280	6.90	1.35	35°	57%	SC-FF
B2	260	25.9	460	4.0	1478	739	12.7	9.56	834	12.36	1390	8.10	1.53	37°	69%	SC-FF
B3	65	6.5	262	2.3	519	259.5	4.5	4.25	375	5.21	507	3.79	1.37	42°	50%	DT
B4	400	35.8	678	5.0	1540	770	11.3	7.88	498	8.09	1319	5.64	1.43	31°	56%	SC-FF
B5	100	9.0	600	4.4	1485	742.5	10.9	10.01	748	10.10	1380	8.84	1.14	32°	60%	SC-FF
B6	75	6.7	300	2.2	495	247.5	3.6	4.31	292	4.39	480	3.91	1.12	45°	39%	DT
B7	60	6.0	260	2.2	630	315	5.4	7.47	410	8.03	600	5.86	1.37	56°	59%	DC
B8	40	3.6	291	2.1	700	350	5.1	7.05	368	8.15	690	6.75	1.21	57°	58%	DC

Notes: P_{cr} = initial flexural crack load. Flexural cracking strength (σ_{cr}) is calculated by $\sigma_{cr} = \frac{M_{cr}}{bh^2/6}$. M_{cr} = bending moment of initial flexural crack $= \frac{P_{cr} \cdot a}{2}$. P_{ci} = initial diagonal crack load. Diagonal cracking strength (v_{ci}) is calculated by $v_{ci} = \frac{P_{ci}/2}{bh_0}$. P_u = ultimate load. V_u = ultimate shear load = $P_u/2$. Ultimate shear strength (τ_u) is calculated as: $\tau_u = V_u/bh_0$, where b is the beam breadth and h_0 is the effective depth of the beam. Δ_u = midspan deflection of ultimate load. PCSR indicates the post-cracking shear resistance, which is calculated by $PSCR = \frac{V_u - V_{ci}}{V_u} \times 100\%$, where $V_{ci} = P_{ci}/2$. $P_{failure}$ = failure load, which indicates the load for the beam to incur significant damage. $\Delta_{failure}$ = midspan deflection of failure load. P_y = yield load. Δ_y = midspan deflection of yield load. The ductility coefficient (μ_Δ) is calculated as: $\mu_\Delta = \Delta_{failure}/\Delta_y$. The symbol θ denotes the angle between the axis of the beam and the critical shear diagonal crack. FF indicates flexural failure.

3.3. Load-Displacement Relationships

Figure 9 displays the load-mid span deflection curves for all tested beams, presenting results for specimens with varying beam heights and steel fiber volume contents. As shown in Figure 9, the load-midspan deflection curves for the specimens initially displayed a nonlinear growth, followed by a sudden drop upon reaching the ultimate load. No significant yielding phase was observed. It is noteworthy that the midspan deflections of the ultimate load (Δ_u) for the U-H35-S0-V2.0 and U-H40-S0-V2.0 beams were reduced by 21.2% and 21.3%, respectively, compared to the U-H35-S0-V1.5 and U-H40-S0-V1.5 beams, as depicted in Figure 8a,b. These results suggest that appropriately reducing the volume content of steel fiber can enhance the ductility of non-stirrup UHPC beams.

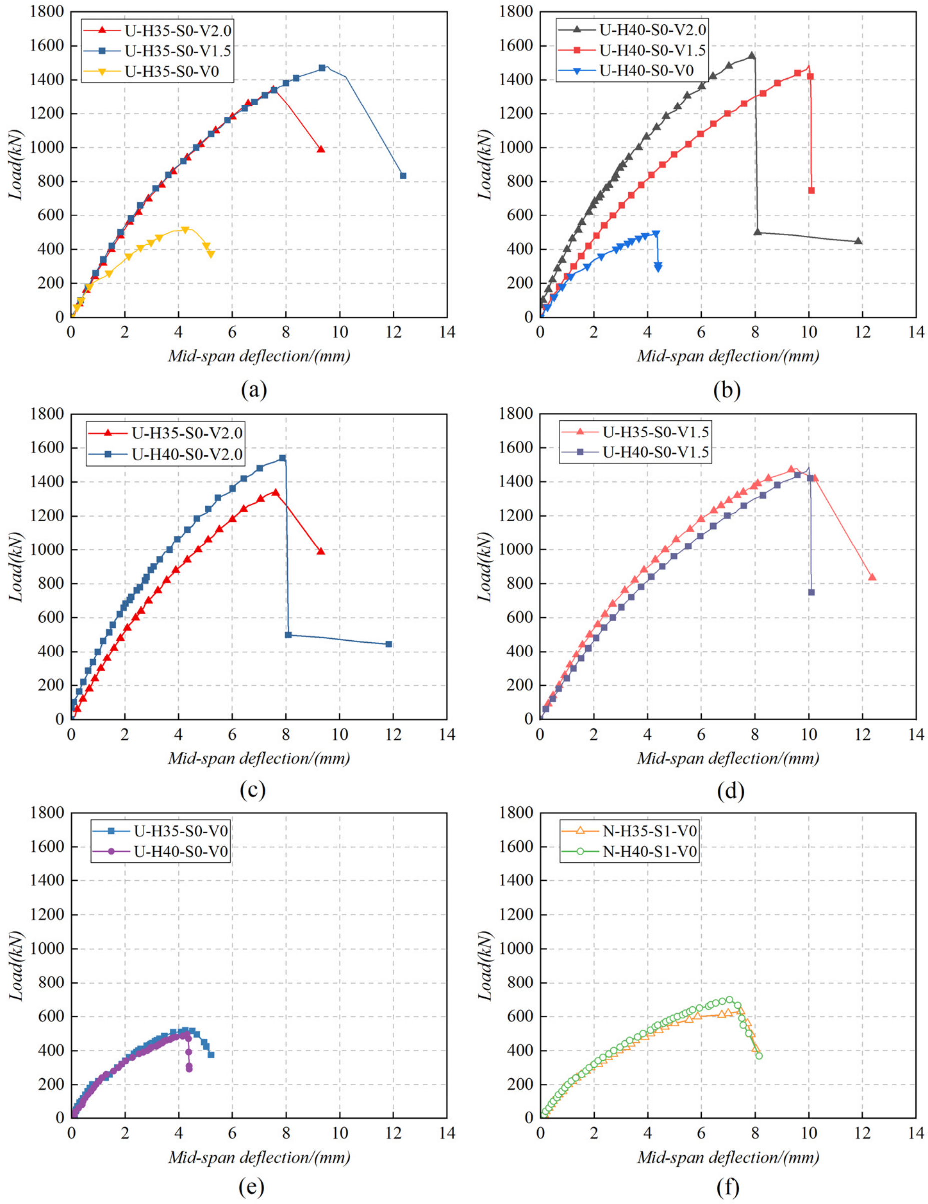

Figure 9. Load-midspan deflection curves. (**a**) Effect of volume content of steel fiber on 350 mm high UHPC beams without stirrup reinforcement; (**b**) effect of volume content of steel fiber on 400 mm high UHPC beams without stirrup reinforcement; (**c**) effect of beam height at a volume content of steel fiber of 2%; (**d**) effect of beam height at a volume content of steel fiber of 1.5%; (**e**) effect of beam height at a volume content of steel fiber of 0%; (**f**) effect of beam height of stirrup-reinforced NC beams.

3.4. Strain Response

3.4.1. Strain Response of Longitudinal Reinforcements

The load–strain relationships of the longitudinal reinforcement for the U-H35-S0-V*, U-H40-S0-V*, and N-H*-S1-V0 beams are illustrated in Figure 10a–c. Some strain gauges adhering to the longitudinal reinforcements were inadvertently damaged at the test's onset due to their susceptibility to damage within the concrete. In these instances, a suitable strain gauge was selected from the pre-embedded strain gauges to assess the strains of the longitudinal reinforcements as detailed in the caption of Figure 10. The yield strength and elastic modulus of the reinforcements were assumed to be 419.2 MPa and 2.0×10^5 MPa, respectively. Consequently, the yield strain of the longitudinal reinforcements was approximately 2096 $\mu\varepsilon$, denoted by the vertical dashed line.

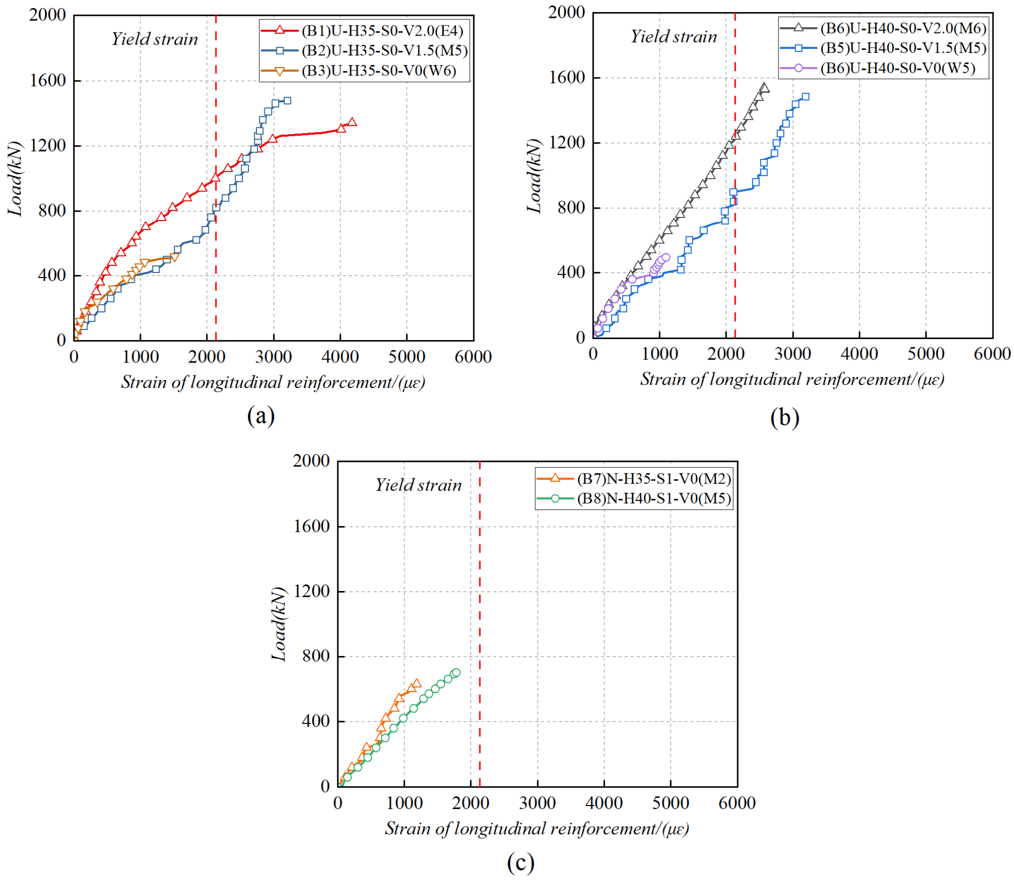

Figure 10. Load–strain curves of longitudinal reinforcements. (**a**) U-H35-S0-V* beams; (**b**) U-H40-S0-V* beams; (**c**) N-H*-S1-V0 beams.

Figure 10a,b show that the longitudinal reinforcement strains for B1 and B2 as well as B4 and B5 reached the yield strain before reaching the ultimate load. However, the longitudinal reinforcement strains for B3 and B6 were far from yielding when they reached the ultimate load, indicating that the lack of steel fibers caused them to fail quickly, far from bending failure after diagonal cracks emerged. It is important to note that as the load increased, the longitudinal reinforcement strains of beams B1, B2, B4, and B5 significantly exceeded the yield strain, suggesting that these beams may have experienced flexural failure. This could explain the abnormal load-bearing capacity of beams B1, B2, B4, and B5 compared to their normal shear capacity. As seen in Figure 10c, the longitudinal reinforcements for B7 and B8 had not yielded either when the ultimate load was reached. For the U-H35-S0-V2.0 and U-H40-S0-V2.0 beams, the loads at which the longitudinal reinforcements yielded increased by up to 22.0% and 37.9%, respectively, compared to beams U-H35-S0-V1.5 and U-H40-S0-V1.5. These findings suggest that the incorporation of steel fibers had indeed improved the strength of UHPC, and that steel fibers could carry the load synergistically with longitudinal reinforcements. Additionally, increasing the steel fiber volume content within a certain range is conducive to enhancing the beams' load-bearing capacity.

3.4.2. Strain Response of Stirrups

The load–strain relationships of the stirrups for beams N-H35-S1-V0 (B7) and N-H40-S1-V0 (B8) are presented in Figure 11. The yield strength and elastic modulus of the stirrup were assumed to be 412 MPa and 2.0×10^5 MPa, respectively. Consequently, the yield strain of the longitudinal reinforcements was approximately 2060 με, which was also marked with a vertical dashed line. As can be observed, the strain of the stirrups in B7 and B8 increased slightly with the increase in load before the diagonal cracks emerged. Upon the emergence of diagonal cracks in the shear-bending section, the strain of the stirrups exhibited a turning point. As the load improved, the strain of the stirrups gradually increased, and finally exceeded the yield strain. The experimental results presented in Figure 11 indicate that the stirrups experienced minimal stress prior to the onset of the diagonal cracks. After the diagonal cracks traversed the shear-bending section, the tensile strength of the concrete in the section was significantly reduced, resulting in the transfer of tensile stress to the stirrups. This is evidenced by the surge in the strain of the stirrups upon the appearance of the diagonal cracks. Furthermore, it is evident that the stirrups in both B7 and B8 yielded before the beams reached their ultimate loads. This suggests that the stirrups were fully utilized in resisting the shear force.

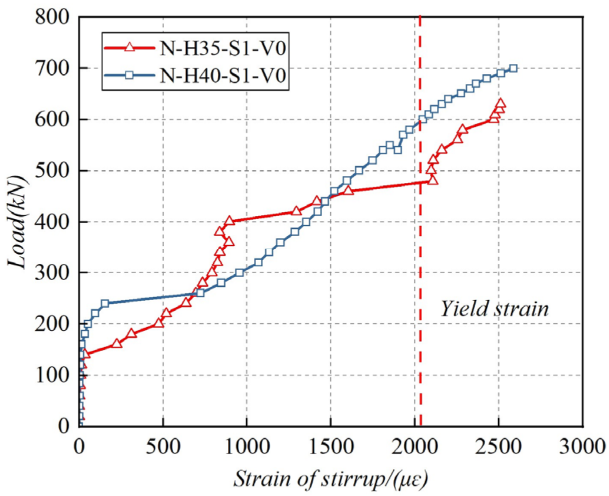

Figure 11. Load–strain curves of stirrups.

3.4.3. Strain Response of Concrete Diagonal Sections

The principal tensile strains ε_t and principal compression strain ε_c were calculated using Equation (1), where ε_x, ε_{45°, and ε_y, and are the strains of strain gauges set at angles of 0°, 45°, and 90°, respectively. The positive calculation results indicate the principal tensile strain, while the negative results indicate the principal compressive strain.

$$\begin{cases} \varepsilon_t \\ \varepsilon_c \end{cases} = \frac{\varepsilon_x + \varepsilon_y}{2} \pm \sqrt{\left(\frac{\varepsilon_x - \varepsilon_y}{2}\right)^2 + \left(\frac{\varepsilon_x + \varepsilon_y}{2} - \varepsilon_{45^\circ}\right)^2} \tag{5}$$

Figure 12 illustrates the load-principal strain relationships of all tested beams, as measured at various points along the diagonal section on the side of failure. Before the diagonal cracks propagated through these strain rosettes, the principal strains on the shear-bending section increased linearly with the applied load. Upon the onset of diagonal cracking in the web section of the beams, there was a sudden surge in principal tensile strains. As diagonal cracks developed, the stresses in the shear-bending section were redistributed, resulting in irregular variations of the principal strains. It is noteworthy that the principal tensile strains on the section of strain rosettes A* to B* exhibited more substantial alterations compared to those on the section of strain rosettes C*. This observation indicates that the concrete in the web section of the tested beams experienced greater tensile stresses than that near the support. Figure 12g,h shows that the principal strains of the normal concrete beams had more pronounced variations than those of the UHPC beams, suggesting that the exceptional tensile properties of UHPC can effectively mitigate concrete cracking.

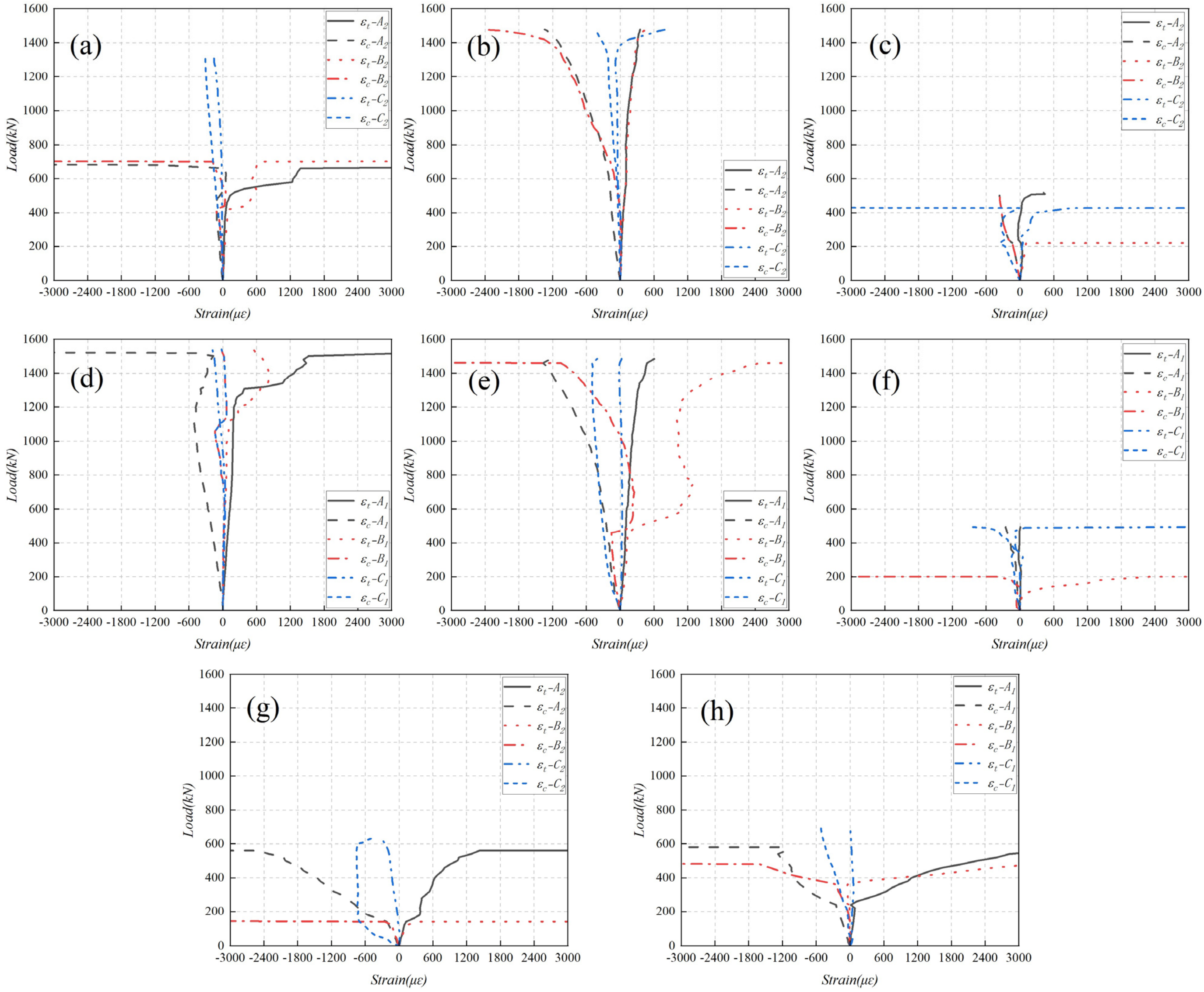

Figure 12. Load-principal stress relationships for concrete diagonal sections. (**a**) B1; (**b**) B2; (**c**) B3; (**d**) B4; (**e**) B5; (**f**) B6; (**g**) B7; (**h**) B8.

3.5. Post-Cracking Shear Resistance

The post-cracking shear resistance (PCSR) of the tested beams is determined by Equation (6), which indicates the load-bearing capacity of the tested beams after the onset of the first shear diagonal crack.

$$PCSR = \frac{V_u - V_{ci}}{V_u} \times 100\% \quad (6)$$

Table 4 lists the calculated values of all tested beams. The average values of PCSR for the U-H*-S0-V2.0, U-H*-S0-V1.5, U-H*-S0-V0, and N-H*-S1-V0 beams were 56.5%, 64.5%, 44.5%, and 58.5%, respectively.

4. Discussion and Analysis of Experimental Results

4.1. Failure Modes and Crack Patterns

4.1.1. Effect of Beam Height on Failure Modes and Crack Patterns

Table 4 lists the initial diagonal crack load (P_{ci}) and the diagonal cracking strength (v_{ci}). It is demonstrated that increasing the beam height (h) could effectively improve the diagonal cracking strength. As the h increased from 350 mm to 400 mm, the v_{ci} could be increased by up to 16.7% (U-H*-S0-V2.0), 30.4% (U-H*-S0-V1.5), 14.5% (U-H*-S0-V0), and 11.9% (N-H*-S1-V0). However, it should be noted that the ultimate shear strength τ_u of non-stirrup UHPC beams decreased by 2.0% (U-H*-S0-V2.0), 16.6% (U-H*-S0-V1.5), and 22.9% (U-H*-S0-V0) as the h increased from 350 mm to 400 mm.

4.1.2. Effect of Steel Fibers on Failure Modes and Crack Patterns

The bridging action of steel fibers plays a crucial role in determining the post-cracking behavior of UHPC. It inhibits the development of microcracks in the UHPC matrix and withstands tensile stresses, especially after concrete cracking. The schematic of bridging action is depicted in Figure 13. As illustrated in Figure 8a–f, the steel fiber volume content has a significant impact on the failure modes of UHPC beams. For example, by comparing specimens B1, B2, and B3 as well as B4, B5, and B6 with the same beam height, respectively, it can be identified that the lack of the bridging action of steel fibers resulted in specimens B3 and B6 quickly losing their load-bearing capacity and suddenly failing. However, in comparison with B3 and B6, the steel fiber-reinforced specimens B1, B2, B4, and B5 demonstrated excellent ductility. The test results confirmed the role of steel fibers in improving the shear resistance of non-stirrup UHPC beams. This finding is in accordance with the experimental results of Li et al. [50], although the ductility coefficients of the UHPC beams in this study were lower than those of the aforementioned study. This discrepancy may be attributed to the differing shear span-to-effective depth and reinforcement ratio between this study and that of Li et al. [50].

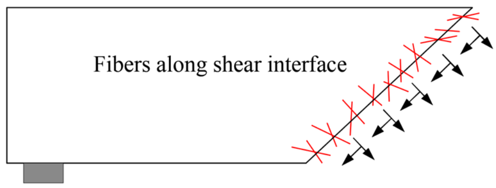

Figure 13. Bridging action from fibers.

Table 4 shows a positive correlation between the volume content of steel fiber and diagonal cracking strength. In the U-H35-S0-V1.5(2.0) and U-H40-S0-V1.5(2.0) beams, the diagonal cracking strength could be increased by up to 81.8%, 127.3%, 109.5%, and 138.1%, respectively, in comparison to the N-H35-S1-V0 and N-H40-S1-V0 beams. In comparison to the U-H35-S1-V0 and U-H40-S1-V0 beams, the incorporation of steel fibers demonstrated a notable enhancement in diagonal cracking strength, with an increase of 73.9%, 117.4%, 100.0%, and 127.3%, respectively. In the U-H35-S0-V2.0 and U-H40-S0-V2.0 beams, the diagonal cracking strength was increased by up to 25.0% and 13.6%, respectively, compared to the U-H35-S0-V1.5 and U-H40-S0-V1.5 beams. The details of the effect of steel fibers on the diagonal cracking strength are shown in Figure 14. From the results, it can be inferred that the incorporation of steel fibers is conducive to delaying diagonal cracking and that an increase in the volume content of steel fiber within a certain range is beneficial for enhancing the beams' diagonal cracking strength.

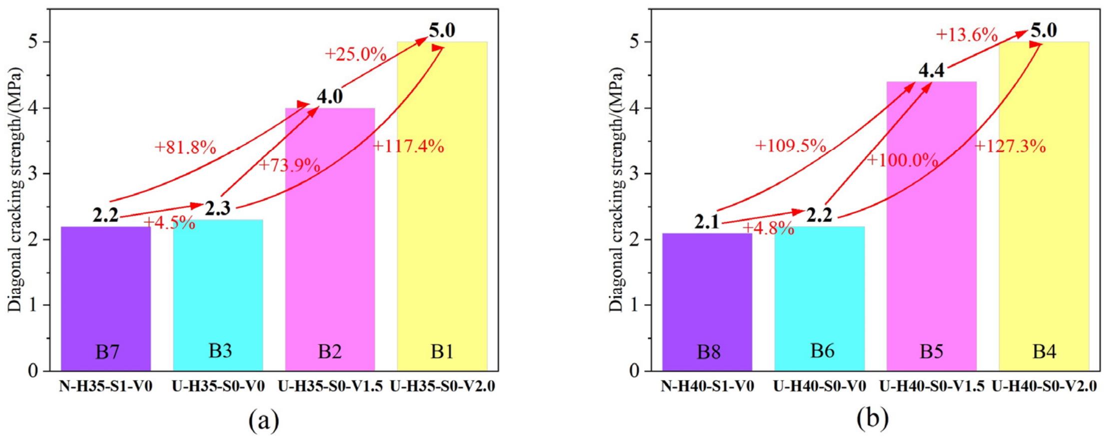

Figure 14. Effect of steel fibers on diagonal cracking strength. (**a**) Effect of steel fibers on diagonal cracking strength of 350 mm high beams; (**b**) effect of steel fibers on diagonal cracking strength of 400 mm high beams.

4.2. Post-Cracking Shear Resistance

The calculated values of PCSR listed in Table 4 suggest that the U-H*-S0-V2.0 (1.5) beams had comparable PCSR to the N-H*-S1-V0 beams. Additionally, in the U-H*-S0-V2.0 beams, PCSR reduced by 8% compared to the U-H*-S0-V1.5 beams, and in the U-H*-S0-V0 beams, PCSR reduced by 14% compared to the N-H*-S1-V0 beams. This indicates that the U-H*-S0-V0 beams cannot achieve comparable PCSR to the N-H*-S1-V0 beams. In the U-H35-S0-V* beams, PCSR increased by 13.5% compared to the U-H40-S0-V* beams. Based on the results presented above, it can be concluded that the incorporation of steel fibers provides non-stirrup UHPC beams with comparable PCSR to NC beams. By reducing the volume content of steel fiber to a certain extent, the PCSR of non-stirrup UHPC beams can be increased to a certain extent. In addition, PCSR increases as the beam height is reduced.

5. Shear Design Recommendations for UHPC Beams

5.1. French Standard Formulae

According to French standard NF P 18-710-2016 [46], the shear capacity of UHPC beams is primarily composed of three resistance terms: the contributions of the UHPC matrix V_c, the stirrup contribution V_s, and the steel fiber contribution V_f. Consequently, the formula for the shear capacity (V_{u1}) of the UHPC beam can be expressed as follows:

$$V_{u1} = V_c + V_S + V_f \tag{7}$$

The formula for the contributions of the UHPC matrix V_c can be described as:

$$V_c = \frac{0.21}{\gamma_{cf}\gamma_E} k_1 \sqrt{f_{cu}} b h_0 \tag{8}$$

where the comprehensive safety factor $\gamma_{cf}\gamma_E$ is set to 1.0. The prestressing improvement factor k_1 was equal to 1.0, since no prestressing was applied to the tested beams in this study.

The contribution of the stirrups V_s is calculated using the following equation:

$$V_s = \frac{A_{sv}}{s} z f_{ys} \cot\theta \tag{9}$$

where A_{sv} denotes the cross-sectional area of the stirrups, s represents the spacing of the stirrups, z is given by $z = 0.9h_0$ to determine the lever arm of internal forces, and f_{ys} indicates the stirrup yielding strength. It was assumed that the non-stirrup UHPC beams tested in this study had no shear contribution from stirrups.

The formula for calculating the contribution of steel fibers V_f can be described as:

$$V_f = A_b \sigma_{f1} \cot\theta \tag{10}$$

where A_b denotes the effective cross-sectional area of the beam, which is equivalent to the value of bz.

5.2. PCI-2021 Formulae

According to the PCI-2021 report [47], the shear capacity of UHPC beams can be divided into three constitutive terms: the contribution of the tensile strength of UHPC V_{cf}, the contribution of effective prestressing force V_p, and the contribution of shear reinforcement V_s. Consequently, the shear capacity V_{u2} can be calculated as follows:

$$V_{u2} = V_{cf} + V_s + V_p \tag{11}$$

$$V_{cf} = \left(\frac{4 f_{rr}}{3}\right) bz\cot\theta \tag{12}$$

$$V_s = \frac{A_{sv} f_{ys} z\cot\theta}{s} \tag{13}$$

$$\theta = 29^\circ + 3500\varepsilon_s \tag{14}$$

where the longitudinal strain ε_s is limited to values of less than -0.40×10^{-3} under compressive stress and less than 6.0×10^{-3} under tensile stress, which correspond to angles of 27.6° and 50.0°, respectively. To ensure consistency with reality, $\theta = 40^\circ$ in this study. The residual tensile strength (f_{rr}) is demonstrated in Table 2. As the UHPC beams tested in this study did not have any prestressing tendons or stirrups, V_p and V_s were taken as zero.

5.3. Xu's Formulae

Xu's formulae [48] provide empirical equations for the shear capacity of UHPC beams, taking into account the influence of prestressing force, steel fibers, and the shear span-to-depth ratio. Therefore, the shear load capacity V_{u3} of UHPC beams can be determined using the following equations:

$$V_{u3} = V_c + V_s + V_f \tag{15}$$

$$V_c = k_2\left(\frac{2}{\lambda - 0.7} - 0.8\right)\sqrt{f_c}\, b h_0 \tag{16}$$

$$V_s = (0.18 + 0.35\lambda)\rho_s f_{ys} b h_0 \tag{17}$$

$$V_f = (0.99 - 0.12\lambda)\lambda f_t b h_0 \tag{18}$$

$$f_t = 0.0353 f_c \tag{19}$$

where ρ_s denotes the stirrup ratio. When λ is smaller than 1.5, λ is set to 1.5, and when λ is larger than 3.0, λ is set to 3.0. The variable k_2 indicates the prestressing enhancement coefficient. For non-prestressed UHPC beams, k_2 is equal to 1.0, while for prestressed UHPC beams, it is equal to 1.25. As the UHPC beams tested in this study did not have any stirrups, it was assumed that the corresponding shear contribution from the stirrups was negligible.

5.4. Comparison of Calculated Values

Table 5 presents the calculated shear capacity V_{u1} (French standard formulae), V_{u2} (PCI-2021 formulae), and V_{u3} (Xu's formulae), along with the ratios $V_{u1}/V_{u,test}$, $V_{u2}/V_{u,test}$, and $V_{u3}/V_{u,test}$ of the calculated shear capacity to the tested shear capacity. The calculated values of shear capacity displayed in Table 5 are all in units of kN.

Table 5. Comparison between the experimental results and calculated values.

Experimental Results		French Standard Formulae					PCI-2021 Formulae				Xu's Formulae				
NO.	$V_{u,test}$	V_c	V_s	V_f	V_{u1}	$V_{u1}/V_{u,test}$	V_{cf}	V_s	V_{u2}	$V_{u2}/V_{u,test}$	V_c	V_s	V_f	V_{u3}	$V_{u3}/V_{u,test}$
B1	670	156.5	0	420.4	576.9	0.86	898.9	0	898.9	1.34	107.5	0	553.0	660.6	0.99
B2	739	161.6	0	621.4	783.1	1.06	1123.6	0	1123.6	1.52	112.9	0	609.5	722.3	0.98
B3	259.5	133.0	0	0	133.0	0.51	324.6	0	324.6	1.25	86.3	0	0	86.3	0.33
B4	770	183.4	0	574.1	757.5	0.98	1053.4	0	1053.4	1.37	126.0	0	648.1	774.1	1.01
B5	742.5	189.4	0	878.2	1067.6	1.44	1316.7	0	1316.7	1.77	132.3	0	714.2	846.5	1.14
B6	247.5	155.9	0	0	155.9	0.63	380.4	0	380.4	1.54	101.1	0	0	101.1	0.41
				Average:		0.91		Average:		1.47			Average:		0.81
				STDEV:		0.33		STDEV:		0.19			STDEV:		0.35
				CV:		0.36		CV:		0.12			CV:		0.43

For the French standard formulae, the ratio $V_{u1}/V_{u,test}$ ranged from 0.51 to 1.44, with a mean of 0.91, an STDEV of 0.33, and a coefficient of variation of 0.36. Comparison with Li et al.'s [50] experimental findings suggested that the formulae were more accurate for UHPC beams with larger shear span–depth ratios. In addition, the average ratio of the calculated shear capacity to the tested shear capacity for the French standard formulae was closest to 1.00.

The ratio of $V_{u2}/V_{u,test}$ for the PCI-2021 formulae ranged from 1.25 to 1.77, with an average of 1.47, a STDEV of 0.19, and a coefficient of variation of 0.12. It was discovered that the calculated values of the PCI-2021 formulae were about 1.5 times the tested results. This demonstrates that the PCI-2021 formulae greatly overestimated the shear capacity of the UHPC beams with larger shear span–depth ratios. Additionally, this phenomenon was more apparent when the beam height was 400 mm.

For Xu's formulae, the ratio $V_{u3}/V_{u,test}$ ranged from 0.33 to 1.14, with an average of 0.81, a STDEV of 0.35, and a coefficient of variation of 0.43. It was found that Xu's formulae significantly underestimated the shear capacity of non-steel fiber-reinforced UHPC beams. Comparison with Li et al.'s [50] experimental findings indicated that Xu's formulae were more accurate for UHPC beams with larger shear span–depth ratios. Moreover, they were more accurate in predicting the shear capacity of steel fiber-reinforced UHPC beams rather than non-steel fiber-reinforced UHPC beams.

The comparison of the calculated values derived from the three formulae demonstrates that the French standard formulae were more accurate for UHPC beams with larger shear span–depth ratios, the PCI-2021 formulae greatly overestimated the shear capacity of UHPC beams with larger shear span–depth ratios, and Xu's formulae were more accurate for steel fiber-reinforced UHPC beams with larger shear span–depth ratios. In summary, the French standard formulae were the most suitable formulae for predicting the shear capacity of UHPC beams in this paper.

6. Conclusions

This study investigated the shear behavior of both non-stirrup UHPC beams and stirrup-reinforced NC beams under a larger shear span–depth ratio (2.8), subjected to three-point loading. The following conclusions can be drawn from the findings:

(1) The failure modes of all eight tested beams were shear failures. Steel fibers are a crucial factor that affects the failure mode of non-stirrup UHPC beams and can effectively enhance the crack resistance of the beam.

(2) Increasing the beam height from 350 mm to 400 mm can effectively improve the diagonal cracking strength. The incorporation of steel fibers is conducive to delaying the appearance of diagonal cracks, and increasing the volume content of steel fibers from 1.5% to 2.0% is beneficial to improving the diagonal cracking strength.

(3) The ductility of non-stirrup UHPC beams can be improved as the volume content of steel fibers decreases from 2.0% to 1.5%.

(4) The concrete of the web section of the tested beams experienced more significant tensile stresses than the concrete near the support. The principal strains of the normal concrete beams had more pronounced variations than those of the UHPC beams.
(5) The ultimate shear strength τ_u of non-stirrup UHPC beams decreased by 2.0% (U-H*-S0-V2.0), 16.6% (U-H*-S0-V1.5), and 22.9% (U-H*-S0-V0) as the beam height increased from 350 mm to 400 mm. The ultimate shear strength τ_u will decrease as the beam height of the beam increases.
(6) PCSR increased by 13.5% as the beam height was reduced from 400 mm to 350 mm. By reducing the volume content of the steel fiber from 2.0% to 1.5%, the PCSR of the non-stirrup UHPC beams can be increased by 8%.
(7) The French standard formulae were more accurate for the UHPC beams with a larger shear span–depth ratio (2.8), the PCI-2021 formulae greatly overestimated the shear capacity of UHPC beams with a larger shear span–depth ratio (2.8), and Xu's formulae were more accurate for steel fiber-reinforced UHPC beams with a larger shear span–depth ratio (2.8). Therefore, the French standard formulae were the most suitable formulae for predicting the shear capacity of UHPC beams in this paper.

Author Contributions: Conceptualization, H.J. and Y.T.; Methodology, L.Z., J.X. and H.J.; Software, L.Z. and B.D.; Validation, L.Z., B.D. and H.J.; Formal analysis, L.Z. and B.H.; Investigation, H.J., L.Z. and B.H.; Resources, H.J.; Data curation, L.Z.; Writing—original draft preparation, L.Z. and B.D.; Writing—review and editing, L.Z. and H.J.; Visualization, L.Z.; Supervision, J.F. and H.J.; Project administration, H.J.; Funding acquisition, H.J. All authors have read and agreed to the published version of the manuscript.

Funding: This research was funded by the National Natural Science Foundation of China with the grant numbers of 51778150 and 52208156.

Data Availability Statement: The original contributions presented in the study are included in the article, further inquiries can be directed to the corresponding authors.

Acknowledgments: This project was undertaken at the plant of the Zhonglu Dura International Engineering Co., Ltd. in Zhaoqing China and the Structural Laboratory of Guangdong University of Technology in Guangzhou, China. The authors would like to acknowledge this generous support.

Conflicts of Interest: Author Yueqiang Tian was employed by the company Zhonglu Xincai (Guangzhou) Technology Co., Ltd. Author Junfa Fang was employed by the company Zhonglu Dura International Engineering Co., Ltd. The remaining authors declare that the research was conducted in the absence of any commercial or financial relationships that could be construed as a potential conflict of interest.

References

1. Wille, K.; Naaman, A.E.; Parra-Montesinos, G.J. Ultra-High Performance Concrete with Compressive Strength Exceeding 150 MPa (22 ksi): A Simpler Way. *ACI Mater. J.* **2011**, *108*, 46.
2. Habel, K.; Viviani, M.; Denarié, E.; Brühwiler, E. Development of the mechanical properties of an ultra-high performance fiber reinforced concrete (UHPFRC). *Cem. Concr. Res.* **2006**, *36*, 1362–1370. [CrossRef]
3. Meng, Q.; Wu, C.; Li, J.; Liu, Z.; Wu, P.; Yang, Y.; Wang, Z. Steel/basalt rebar reinforced Ultra-High Performance Concrete components against methane-air explosion loads. *Compos. Part B Eng.* **2020**, *198*, 108215. [CrossRef]
4. Fang, H.; Gu, M.; Zhang, S.; Jiang, H.; Fang, Z.; Hu, J. Effects of Steel Fiber and Specimen Geometric Dimensions on the Mechanical Properties of Ultra-High-Performance Concrete. *Materials* **2022**, *15*, 3027. [CrossRef]
5. Cuenca, E.; Postolachi, V.; Ferrara, L. Cellulose nanofibers to improve the mechanical and durability performance of self-healing Ultra-High Performance Concretes exposed to aggressive waters. *Constr. Build. Mater.* **2023**, *374*, 130785. [CrossRef]
6. Lee, M.G.; Wang, Y.C.; Chiu, C.T. A preliminary study of reactive powder concrete as a new repair material. *Constr. Build. Mater.* **2007**, *21*, 182–189. [CrossRef]
7. Zhou, M.; Lu, W.; Song, J.; Lee, G.C. Application of ultra-high performance concrete in bridge engineering. *Constr. Build. Mater.* **2018**, *186*, 1256–1267. [CrossRef]
8. Xue, J.; Briseghella, B.; Huang, F.; Nuti, C.; Tabatabai, H.; Chen, B. Review of ultra-high performance concrete and its application in bridge engineering. *Constr. Build. Mater.* **2020**, *260*, 119844. [CrossRef]
9. Zhu, Y.; Zhang, Y.; Hussein, H.H.; Chen, G. Flexural strengthening of reinforced concrete beams or slabs using ultra-high performance concrete (UHPC): A state of the art review. *Eng. Struct.* **2020**, *205*, 110035. [CrossRef]

10. Feng, J.; Shao, X.; Qiu, M.; Li, H.; Gao, X.; Huang, Z. Reliability evaluation of flexural capacity design provision for UHPC beams reinforced with steel rebars/prestressing tendons. *Eng. Struct.* **2024**, *300*, 117160. [CrossRef]
11. Cao, Z.; Li, Z.; Deng, S.; Wang, L.; Jiang, H.; Xian, B. Experimental study on interfacial shear behavior of PBL shear connector deeply embedded in UHPC. *Case Stud. Constr. Mater.* **2023**, *18*, e02192. [CrossRef]
12. Aaleti, S.; Petersen, B.; Sritharan, S. *Design Guide for Precast UHPC Waffle Deck Panel System, Including Connections*; United States Department of Transportation Federal Highway Administration: Washington, DC, USA, 2013.
13. Voo, Y.L.; Foster, S.J.; Voo, C.C. Ultrahigh-performance concrete segmental bridge technology: Toward sustainable bridge construction. *J. Bridge Eng.* **2015**, *20*, B5014001. [CrossRef]
14. Hu, Z.; Xu, Z.; Zhang, S.; Jiang, H.; Chen, Y.; Xiao, J. Experimental study on shear behavior of precast high-strength concrete segmental beams with external tendons and dry joints. *Buildings* **2022**, *12*, 134. [CrossRef]
15. Feng, J.; Fang, S.; Chen, M.; Fang, Z.; Liang, W. Effect of joint width on shear behaviour of wet joints using reactive powder concrete with confining stress. *Eng. Struct.* **2023**, *293*, 116566. [CrossRef]
16. Jiang, H.; Huang, C.; Mei, G.; Gao, X.; Tian, Y.; Sun, X. Experimental and numerical investigations on direct shear performance of UHPC dry joints. *Eng. Struct.* **2023**, *283*, 115872. [CrossRef]
17. Chen, M.; De Corte, W.; Jiang, H.; Taerwe, L. Experimental study on direct-shear behaviour of narrow joints in socket connections for precast pier-to-pile footing systems. In *Structures*; Elsevier: Amsterdam, The Netherlands, 2024; Volume 61, p. 106006.
18. Jiang, H.; Dong, X.; Fang, Z.; Xiao, J.; Chen, Y. Experimental study on shear behavior of a UHPC connection between adjacent precast prestressed concrete voided beams. *J. Bridge Eng.* **2020**, *25*, 04020106. [CrossRef]
19. Jiang, H.; Hu, Z.; Feng, J.; Wang, T.; Xu, Z. Flexural behavior of UHPC-filled longitudinal connections with non-contacting lap-spliced reinforcements for narrow joint width. In *Structures*; Elsevier: Amsterdam, The Netherlands, 2022; Volume 39, pp. 620–636.
20. Fang, Z.; Wu, J.; Zhao, G.; Fang, S.; Ma, Y.; Jiang, H. Shear performance and design recommendations of single embedded nut bolted shear connectors in prefabricated steel–UHPC composite beams. *Steel Compos. Struct.* **2024**, *50*, 319–336.
21. Fang, Z.; Wu, J.; Xu, X.; Ma, Y.; Fang, S.; Zhao, G.; Jiang, H. Grouped rubber-sleeved studs–UHPC pocket connections in prefabricated steel–UHPC composite beams: Shear performance under monotonic and cyclic loadings. *Eng. Struct.* **2024**, *305*, 117781. [CrossRef]
22. Fang, Z.; Fang, H.; Huang, J.; Jiang, H.; Chen, G. Static behavior of grouped stud shear connectors in steel–precast UHPC composite structures containing thin full-depth slabs. *Eng. Struct.* **2022**, *252*, 113484. [CrossRef]
23. Fang, Z.; Fang, H.; Li, P.; Jiang, H.; Chen, G. Interfacial shear and flexural performances of steel–precast UHPC composite beams: Full-depth slabs with studs vs. demountable slabs with bolts. *Eng. Struct.* **2022**, *260*, 114230. [CrossRef]
24. Fang, Z.; Liang, W.; Fang, H.; Jiang, H.; Wang, S. Experimental investigation on shear behavior of high-strength friction-grip bolt shear connectors in steel-precast UHPC composite structures subjected to static loading. *Eng. Struct.* **2021**, *244*, 112777. [CrossRef]
25. Xiao, J.; Zeng, H.; Huang, H.; Liu, L.; Li, L.; Yuan, B.; Zhong, Z. Experimental Investigation on the Influence of Strength Grade on the Surface Fractal Dimension of Concrete under Sulfuric Acid Attack. *Buildings* **2024**, *14*, 713. [CrossRef]
26. Xiao, J.; Huang, L.; He, Z.; Qu, W.; Li, L.; Jiang, H.; Zhong, Z.; Long, X. Probabilistic models applied to concrete corrosion depth prediction under sulfuric acid environment. *Measurement* **2024**, *234*, 114807. [CrossRef]
27. Cai, Z.W.; Yu, J.T.; Duan, X.Z.; Deng, B.Y.; Lu, Z.D.; Yu, K.Q. Enhancing the strain-hardening performance of ultra-high performance concrete by tailoring matrix toughness and fiber parameters. *Constr. Build. Mater.* **2023**, *395*, 132335. [CrossRef]
28. Yu, R.; Fan, D.Q.; Sun, M.J.; Zhang, J.J.; Shui, Z.H.; Hou, D.S.; Wang, D.S.; Wang, X.P.; Feng, Y. Effects of steel fibre content 3D network on performance of ultra-high performance concrete. *J. Chin. Ceram. Soc.* **2021**, *49*, 2313–2321.
29. Qi, J.; Ma, Z.J.; Wang, J. Shear strength of UHPFRC beams: Mesoscale fiber-matrix discrete model. *J. Struct. Eng.* **2017**, *143*, 04016209. [CrossRef]
30. Abbas, Y.M.; Iqbal Khan, M. Influence of fiber properties on shear failure of steel fiber reinforced beams without web reinforcement: ANN modeling. *Lat. Am. J. Solids Struct.* **2016**, *13*, 1483–1498. [CrossRef]
31. Amin, A.; Gilbert, R.I. Instantaneous crack width calculation for steel fiber-reinforced concrete flexural members. *ACI Struct. J.* **2018**, *115*, 535–543. [CrossRef]
32. Meng, W.; Khayat, K.H. Effect of hybrid fibers on fresh properties, mechanical properties, and autogenous shrinkage of cost-effective UHPC. *J. Mater. Civ. Eng.* **2018**, *30*, 04018030. [CrossRef]
33. Ding, Y.; You, Z.; Jalali, S. The composite effect of steel fibres and stirrups on the shear behaviour of beams using self-consolidating concrete. *Eng. Struct.* **2011**, *33*, 107–117. [CrossRef]
34. Jiang, H.; Hu, Z.; Cao, Z.; Tian, Y.; Sun, X. Experimental and numerical study on shear performance of externally prestressed precast UHPC segmental beams without stirrups. In *Structures*; Elsevier: Amsterdam, The Netherlands, 2022; Volume 46, pp. 1134–1153.
35. Lee, J.W.; Joh, C.; Choi, E.S.; Kwak, I.J.; Kim, B.S. Estimation of Shear Behavior of Ultra High Performance Concrete I Girder without Shear Stirrups. *Key Eng. Mater.* **2013**, *525*, 557–560.
36. Voo, Y.L.; Foster, S.J.; Gilbert, R.I. Shear strength of fiber reinforced reactive powder concrete prestressed girders without stirrups. *J. Adv. Concr. Technol.* **2006**, *4*, 123–132. [CrossRef]
37. Voo, Y.L.; Poon, W.K.; Foster, S.J. Shear strength of steel fiber-reinforced ultrahigh-performance concrete beams without stirrups. *J. Struct. Eng.* **2010**, *136*, 1393–1400. [CrossRef]

38. Yang, I.H.; Joh, C.; Lee, J.W.; Kim, B.S. An experimental study on shear behavior of steel fiber-reinforced ultra high performance concrete beams. *KSCE J. Civ. Environ. Eng. Res.* **2012**, *32*, 55–64.
39. Ahmad, S.; Bahij, S.; Al-Osta, M.A.; Adekunle, S.K.; Al-Dulaijan, S.U. Shear behavior of ultra-high-performance concrete beams reinforced with high-strength steel bars. *ACI Struct. J.* **2019**, *116*, 3–14. [CrossRef]
40. El-Sayed, A.K.; El-Salakawy, E.F.; Benmokrane, B. Shear strength of fibre-reinforced polymer reinforced concrete deep beams without web reinforcement. *Can. J. Civ. Eng.* **2012**, *39*, 546–555. [CrossRef]
41. Zagon, R.; Matthys, S.; Kiss, Z. Shear behaviour of SFR-UHPC I-shaped beams. *Constr. Build. Mater.* **2016**, *124*, 258–268. [CrossRef]
42. Baby, F.; Marchand, P.; Toutlemonde, F. Shear behavior of ultrahigh performance fiber-reinforced concrete beams. I: Experimental investigation. *J. Struct. Eng.* **2014**, *140*, 04013111. [CrossRef]
43. Pourbaba, M.; Joghataie, A.; Mirmiran, A. Shear behavior of ultra-high performance concrete. *Constr. Build. Mater.* **2018**, *183*, 554–564. [CrossRef]
44. Zhou, J.; Wu, W.; Caprani, C.C.; Tan, Z.; Wei, B.; Zhang, J. A hybrid virtual-real traffic simulation approach to reproducing the spatiotemporal distribution of bridge loads. *Comput.-Aided Civ. Infrastruct. Eng.* 2024. [CrossRef]
45. Feng, J.; Li, P.; Wu, J.; Jiang, H.; Tian, Y.; Sun, X. Shear behavior of externally prestressed UHPC beams without stirrups. *Case Stud. Constr. Mater.* **2023**, *18*, e01766. [CrossRef]
46. *NF P18-710*; National Addition to Eurocode 2—Design of Concrete Structures: Specific Rules for Ultra-High Performance Fibre-Reinforced Concrete (UHPFRC). French Standardization Association: Paris, France, 2016.
47. Tadros, M.; Lawler, J.; El-Khier, M.A.; Gee, D.; Kurt, A.; Lucier, G.; Wagner, E. *Implementation of Ultra-High-Performance Concrete in Long-Span Precast Pretensioned Elements for Concrete Buildings and Bridges*; Precast/Prestressed Concrete Institute (PCI): Chicago, IL, USA, 2021.
48. Xu, H.B.; Deng, Z.C.; Chen, C.S.; Chen, X.W. Experimental study on shear strength of ultra-high performance fiber reinforced concrete beams. *China Civ. Eng. J.* **2014**, *47*, 91–97.
49. Yalciner, H.; Kumbasaroglu, A.; Ergun, U. Effects of geo-grid and conventional stirrups on reinforced concrete beams with polypropylene fibers. In *Structures*; Elsevier: Amsterdam, The Netherlands, 2018; Volume 13, pp. 230–242.
50. Li, P.; Cheng, Q.; Chen, N.; Tian, Y.; Fang, J.; Jiang, H. Experimental Study on Shear Behavior of Non-Stirrup Ultra-High Performance Concrete Beams. *Materials* **2023**, *16*, 4177. [CrossRef]